Multi-Task Learning Convolutional Neural Network and Optical Spectrums Enabled Optical Performance Monitoring

Chenglong Yu, Haoyu Wang, Changjian Ke, Zi Liang, Sheng Cui, and Deming Liu

***Abstract*—We propose a simultaneous optical signal recognition (OSR) and optical signal-to-noise ratio (OSNR) monitoring method by using multi-task learning convolutional neural network (MTL-CNN) in conjunction with optical spectrums, which enables optical performance monitoring (OPM) in the optical transmission network. In order to achieve a trade-off between monitoring loss and time consumption of the MTL-CNN constructed for seven commonly used signals with a spectrum resolution of 10 pm, the number of feature map channels in four convolutional layers is delicately designed as 32, 32, 64, and 64 with task weights set to 0.4 and 0.2, corresponding to OSNR monitoring and OSR, respectively. Simulation results manifest that this method can realize the recognition of the received optical signals with an overall accuracy of 100% and also enable OSNR monitoring with the mean absolute error (MAE) of 0.262 dB. The proposed method shows strong robustness to various distortions and exhibits good performance in terms of time consumption. The effectiveness is further verified by proof-of-concept experiments in three signals. These illustrate that our method is a promising solution for multi-parameter monitoring with high accuracy and efficiency.**

***Index Terms*—Optical spectrum, convolutional neural network, multi-task learning, optical performance monitoring, optical signal recognition, optical signal-to-noise ratio monitoring.**

I. Introduction

With the development of technologies such as cloud computing, high-definition video, and the Internet of Everything, the capacity of optical network is growing rapidly and elastic optical network (EON) [1], [2] has emerged. Optical performance monitoring (OPM) technology is indispensable for the management of optical networks. Real-time adjustment of the optical signal (OS) type in link transmission according to changes in traffic demand is beneficial for improving spectrum efficiency [3]. Besides, recognizing the OS type in the optical fiber link can also be an effective defense against multiple optical network intrusion attacks [4]. The optical signal-to-noise ratio (OSNR) is directly related to the bit error ratio (BER) and can be used to characterize the signal quality [5], thus playing a key role in link diagnosis [6]. Therefore, OS recognition (OSR) and OSNR monitoring technologies are significant for maintaining the flexible and dynamic operation of optical networks.

Due to the diverse needs of users, optical network architectures become more dynamic, and thus various optical performance parameters are time-varying. To reduce system cost, guarantee optimum resources utilization and ensure proper management of EON, it is significant to monitor various optical performance parameters at the same time. Currently, a plethora of frequency domain, time domain, and polarization domain OSR and OSNR monitoring technologies have been proposed [7]. In the time domain and polarization domain, constellation diagrams [8], eye diagrams [9], and stokes planes [10] have been utilized for OSR. Similarly, OSNR monitoring methods based on asynchronous delay-tap sampling (ADTS) [11], asynchronous single channel sampling (ASCS) [12], waveforms [13], amplitude histograms (AHs) [6] have also been proposed. Recently, there are some other schemes that simultaneously implement OSR and OSNR monitoring based on the dual-stage deep neural network such as schemes presented in [14], [15]. However, the above features are more or less susceptible to chromatic dispersion (CD) or polarization mode dispersion (PMD). For signals with different CD or PMD values, the above features are morphologically different, even if other parameters remain the same. Besides, high-speed coherent receivers or large-bandwidth photodetectors are required, resulting in expensive system hardware costs. The optical spectrum based schemes have received increasing attention due to the large tolerance for dispersion and wide deployment in optical network nodes. In [4], a one-dimensional convolutional neural network (1D-CNN) is demonstrated as a practical tool to accurately recognize OS type under different transmission conditions, but only one OS type is considered. Nine OS types are recognized by combining principal component analysis (PCA) and support vector machine (SVM) [16], but the performance of SVM is poor when dealing with large-scale data set [17]. In [18]–[20], the reference optical spectrum method with the help of prior transmission information realizes in-band OSNR monitoring. Due to the lack

Manuscript received January 13, 2022; revised February 10, 2022; accepted February 19, 2022. Date of publication February 25, 2022; date of current version March 15, 2022. This work was supported by the National Natural Science Foundation of China under Grant 61975063. *(Chenglong Yu and Haoyu Wang contributed equally to this work.) (Corresponding author: Changjian Ke.)*

Chenglong Yu, Haoyu Wang, and Zi Liang are with the School of Optical and Electronic Information, Huazhong University of Science and Technology, Wuhan 430074, China (e-mail: m201972229@hust.edu.cn; wanghaoyu@hust.edu.cn; zilianghust@hust.edu.cn).

Changjian Ke, Sheng Cui, and Deming Liu are with the School of Optical and Electronic Information, Huazhong University of Science and Technology, Wuhan 430074, China, and also with the Wuhan National Laboratory for Optoelectronics, Wuhan 430074, China (e-mail: cjke@mail.hust.edu.cn; cuisheng@hust.edu.cn; dmliu@mail.hust.edu.cn).

Digital Object Identifier 10.1109/JPHOT.2022.3153638

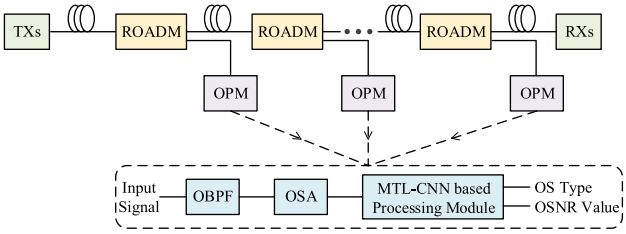

Fig. 1. Schematic diagram of the proposed method. TXs: transmitters, RXs: receivers.

of intelligence, it is not applicable to EON with dynamically variable transmission information. Some machine learning methods, such as SVM [21] and gaussian process regression (GPR) [22], [23] have been used to achieve intelligent OSNR monitoring. However, multiple distortions in the optical fiber link are not taken into account. The above-mentioned techniques based on optical spectrums focus on either OSR or OSNR monitoring. However, it's of great importance to simultaneously realize intelligent OSR and OSNR monitoring in the future elastic and cognitive optical network.

1D-CNN excels in 1D data processing and has the ability to extract local information. Therefore, in this paper, we propose a multi-task learning CNN (MTL-CNN) technique to overcome the above shortcomings, where the classification task is used to perform OSR and the regression task is used to perform OSNR monitoring. We utilize a MTL-CNN and once the training process is finished, the optical spectrum to be analyzed is input to obtain its OS type and OSNR value. After optimizing the model structure and task weights, the simulation results show that the mean absolute error (MAE) of OSNR monitoring is 0.436, 0.262 and 0.101 dB with a spectrum resolution of 20, 10 and 1 pm, respectively, and the recognition accuracy is up to 100% for the seven commonly used signals in the presence of multiple distortions. The monitoring performance is slightly worse in the 20 pm case than in the 10 pm case. With a spectrum resolution of 1 pm, the monitoring performance gets better, but at the cost of more time consumption. Furthermore, proof-of-concept experiments have been implemented to demonstrate the effectiveness of the proposed scheme for joint OSR and OSNR monitoring among three signals. The MAE of OSNR monitoring is 0.317, 0.244 and 0.342 dB with a spectrum resolution of 20, 10 and 1 pm, respectively, and the recognition accuracy remains 100%. All this indicates that our method can realize relatively good multi-parameter monitoring with low time consumption in the presence of distortions.

II. Operating Principle

The proposed OPM technique that can monitor both OS type and OSNR at the intermediate nodes of the optical fiber link is shown in Fig. 1. After the reconfigurable optical add/drop multiplexer (ROADM), signals are tapped for the input of OPM. The optical spectrum to be analyzed is obtained after an optical bandpass filter (OBPF) and optical spectrum analyzer (OSA). Then it will be fed into the MTL-CNN based processing module for simultaneously achieving its OS type and the corresponding OSNR value.

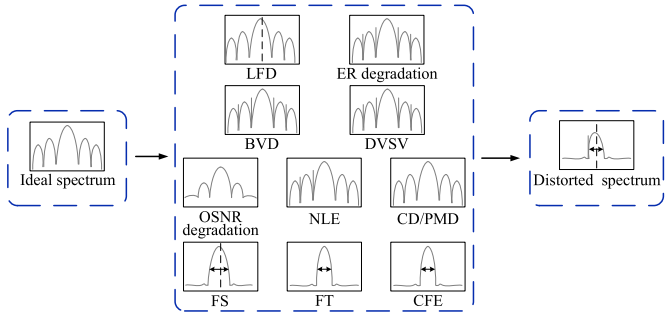

Fig. 2. Schematic diagram of the effects of transmitter and link distortions on the optical spectrum.

A. Optical Spectrum

It is well known that each type of OS has its unique spectrum, and differences in modulation format, baud rate, and pulse shape lead to spectrum variability [24]. The spectrums of on-off keying (OOK) signal have spectral lines with intervals equal to the baud rate, while the spectrums of the signal corresponding to phase-shift keying (PSK) and quadrature amplitude modulation (QAM) such as binary PSK (BPSK), quadrature PSK (QPSK), 8PSK, 16QAM, and 64QAM do not contain similar spectral lines. This is due to the fact that, unlike several other modulation formats, the OOK signal constellations are asymmetric with respect to the origin of the complex plane [24]. It is also found that when the modulation format and pulse shape are determined, the spectrum main lobe width (MLW) is related to the baud rate of the signal, and the larger the baud rate, the larger the MLW. With other factors consistent, the Nyquist-pulse-shaped signals have much narrower MLW. Additionally, the signals with certain combinations of modulation format, baud rate, and pulse shape will have the same spectrum. For example, MPSK and MQAM signals with the same baud rate and pulse shape have the same spectrum theoretically. Therefore, an ideal optical spectrum can be used for distortion analysis of several different signals and this technique is somewhat modulation format independent [16], [25]. The OSNR monitoring method based on reference optical spectrum [18]–[20] considers signals with the same spectrum as a class and uses the corresponding ideal spectrum as a reference spectrum without recognizing which specific OS type it is.

The signals usually experience various distortions at the transmitter and optical fiber link [4], [16]. Taking a QPSK signal as an example, Fig. 2 reveals how its ideal spectrum is influenced by the transmitter and optical fiber link distortions. At the transmitter side, the signals are affected by the laser frequency drift (LFD), which causes an overall shift in the spectrum. During the modulation process, distortions such as bias voltage drift (BVD), drive voltage swing variation (DVSV), extinction ratio degradation (ERD) are caused by non-ideal modulation elements. As soon as optical fiber links are mentioned, fiber loss, CD, PMD, and nonlinear effect (NLE) come into view. With the widespread use of erbium-doped fiber amplifier (EDFA), the fiber loss can be compensated, but at the same time, the amplified spontaneous emission (ASE) noise is introduced, which raises the spectrum noise floor and brings about OSNR degradation.

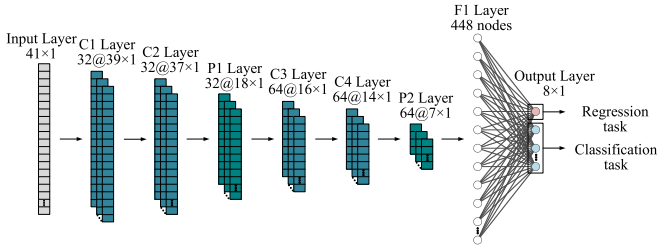

Fig. 3. Schematic diagram of the MTL-CNN model.

Unlike CD and PMD, which have relatively little influence on the spectrum, NLE generates new frequency components that broaden the spectrum slightly. Filter shift (FS) and Filter tightening (FT) caused by non-ideal optical filtering elements noticeably deform the expected shape of the spectrum. Apart from these, the cascaded filtering effect (CFE) resulting from a series of wavelength selective switches (WSSs) has a similar impact on the spectrum as FT.

B. MTL-CNN

As a kind of deep learning, CNN has received widespread attention due to its powerful learning ability. The two-dimensional CNN (2D-CNN) excels in image recognition and 1D-CNN is commonly used for data processing, such as the optical spectrum data in this paper. In practice, in the face of different requirements, it is often necessary to establish corresponding CNN models, such as those implementing classification and regression tasks. MTL facilitates the simultaneous execution of multiple tasks and improves model generalization by sharing domain information implicit in the samples of related tasks [26], [27]. Currently, it has been widely used in fields such as computer vision to improve pattern recognition accuracy [28]. MTL-CNN is a CNN model based on multi-task learning. For different tasks, by connecting specific activation functions to neurons, multiple tasks can be performed simultaneously.

The convolutional layer and pooling layer are two core components of CNN. The convolutional layer consists of a series of convolutional kernels with small receptive fields that generate a feature map by traversing the entire depth of the input data, thus enabling feature extraction. Different convolutional kernels detect different data features and generate the corresponding feature maps to establish an effective model. The pooling layer, which usually follows the convolutional layer, divides the input feature map into smaller blocks and extracts the corresponding features. The pooling operation can effectively guarantee the relative position of features, reduce the dimensionality of the output without increasing the number of parameters to be trained and accelerate the network fitting process.

Fig. 3 shows the MTL-CNN designed for simultaneous OSR and OSNR monitoring in this paper. This model borrows from the classic VGG-like architecture, by using a convolutional layer of multiple smaller convolutional kernels rather than a larger convolutional kernel, which on the one hand reduces the parameters and on the other hand corresponds to a more nonlinear mapping [29], [30]. The optical spectrum sample is represented by a 1D vector $X = [x_1, x_2, \cdots, x_p]$ which consists of p power values corresponding to the frequency sampling grid (e.g., grid size of 50 GHz centered at 1550 nm) and normalized. The pre-processed optical spectrum has been used as input to the model. In our practical system, we set four convolutional layers (C1, C2, C3, C4) with a kernel size of 3×1 to generate 32, 32, 64, and 64 feature maps respectively. Another two pooling layers (P1, P2), where both subsampling regions are 2×1, are also added into the model. The maximum pooling, which takes the largest value of the data in the segmented feature map as the representative of a specific block of features, is used for down-sampling. After the second down-sampling, the output of P2 is mapped into the fully connected layer (F1), consisting of 448 neurons. At last, F1 is fully connected with the output layer, comprising 8 neurons (1 neuron for OSNR monitoring and 7 neurons for OSR). For OSNR monitoring, the actual value should be continuous and thus it is a regression task. While for OSR, the output is discrete and thus belongs to the classification task. The activation functions of the output layer for OSR and OSNR monitoring are Softmax as shown in (1) and linear function respectively, while the activation functions of the other layers adopt rectified linear units (ReLU).

$$Softmax = \frac{e^{x_i}}{\sum_{i}^{m} e^{x_i}} \tag{1}$$

In addition, it is necessary to determine the corresponding loss function according to the type of task. Mean square error (MSE) and cross-entropy are used for regression task and classification task respectively, as shown in (2)(3):

$$L_1 = \frac{1}{m}\sum_{i=1}^{m}(y_i - \hat{y}_i)^2 \tag{2}$$

$$L_2 = -\frac{1}{m}\left[\sum_{i=1}^{m} y_i log\hat{y}_i + (1-y_i)log(1-\hat{y}_i)\right] \tag{3}$$

where m is the number of samples, and y_i, $\hat{y}_i$ are the actual and estimated values, respectively. In order to obtain the total loss function L of the model, the loss functions of different tasks should be weighted and summed, as shown in (4):

$$L = \lambda_1 L_1 + \lambda_2 L_2 \tag{4}$$

where, L_1, L_2 are the MSE loss function and the cross-entropy loss function, respectively, and λ_1, λ_2 are their corresponding weight coefficients. The values of λ_1 and λ_2 will affect the monitoring results of the model. To prevent significant performance differences between different tasks, the weights of the two tasks need to be reasonably adjusted to optimize the overall performance of the model.

III. Numerical Simulations and Results

Numerical simulation based on the commercial simulation tool VPI Transmission Maker 9.5 and MATLAB R2017a has been employed to investigate the performance of the proposed method. Fig. 4 exhibits the system configuration used in our

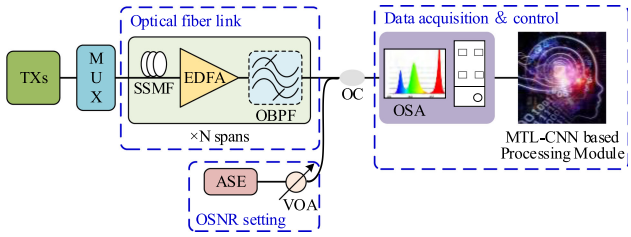

Fig. 4. Schematic diagram of the setup of the simulation system.

TABLE I
THE SEVEN COMMONLY USED SIGNALS AND CORRESPONDING LABELS

Label	OS type
OS1	10 Gbaud 50%RZ-OOK
OS2	10 Gbaud 50%RZ-BPSK
OS3	20 Gbaud NRZ-QPSK
OS4	25 Gbaud PDM-NRZ-QPSK
OS5	28 Gbaud PDM-NRZ-8PSK
OS6	28 Gbaud PDM-Nyquist-16QAM
OS7	35 Gbaud PDM-Nyquist-64QAM

simulation. The signals are launched into the optical fiber link via the wavelength division multiplexer (MUX) with a channel interval of 50 GHz. Each span usually includes an 80 km-long standard single-mode fiber (SSMF), an EDFA, and an OBPF. The attenuation coefficient, dispersion parameter and nonlinear coefficient of SSMF are 0.2 dB/km, 16 ps/nm/km, and 1.3 /km/W, respectively. Fiber loss of each span is compensated by the EDFA. A realistic fourth-order Gaussian multichannel OBPF with 3 dB bandwidth of 50 GHz has been utilized to form FS and CFE. It's noteworthy that it is plotted with a dashed line and may not appear in each span. The signals have already propagated through 24 SSMF spans before reaching the monitoring node. Then through an optical coupler (OC), an additional ASE source is fed into the signals. With the help of a variable optical attenuator (VOA), signals with different OSNR values can be achieved before entering OSA and the MTL-CNN based processing module.

The seven commonly used signals listed in Table I are simulated and their ideal spectrums are displayed in Fig. 5. The selected signals include widely used modulation formats such as OOK, BPSK, QPSK, 8PSK, 16QAM, and 64QAM, involving a variety of pulse shaping methods such as non-return-to-zero (NRZ), return-to-zero (RZ), and Nyquist pulse shaping. Polarization Division Multiplexing (PDM) is also considered. The signal rates range from 10 Gb/s to 420 Gb/s, including the mainstream transmission rates in the existing optical network. Considering a real scenario where multiple distortions are present at the transmitter and optical fiber link as depicted in Table II, 54432 simulation samples are collected in total. In addition, each sample contains 8 neurons to label the corresponding OS type and OSNR value. We set 7 neurons whose value is "1" or "0", to denote the OS type: OS1: 0000001, OS2: 0000010, OS3: 0000100, OS4: 0001000, OS5: 0010000, OS6: 0100000, OS7: 1000000. In contrast, the neuron used to label the OSNR value is continuous. The whole optical spectrum data set is randomly divided into training and testing data set with a ratio of 70% and 30%, respectively. Keras library combined with TensorFlow backend are selected for the establishment of MTL-CNN model due to their high operability and ease of implementation [31]. In order to train the model, the parameters in the network are gradually adjusted with the adaptive moment estimation (Adam) algorithm. During the testing process, the accuracy of OSR and the error of OSNR monitoring are analyzed to validate the performance of the trained model.

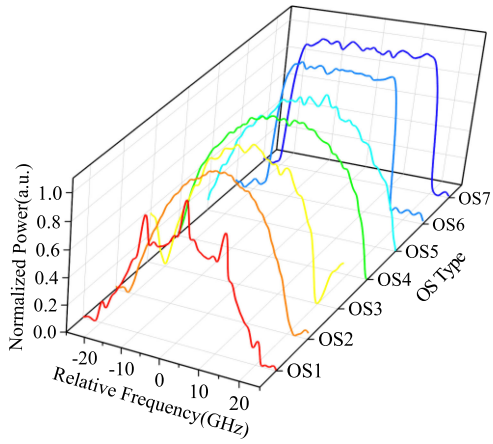

Fig. 5. The ideal spectrums corresponding to the seven commonly used signals.

TABLE II
VARIATION RANGES OF DISTORTIONS

Distortions	Variation ranges
LFD	-0.5,0,0.5 GHz
ER	20,24,28 dB
FS	-2,0,2 GHz
CFE	4,6,8 OBPFs
Power	2,4,6,8 dBm
OSNR	OS1-4:10-17, OS5-6:16-23 OS7:25-32, step=1 dB

In this paper, the effects of task weights and model structure on the performance of MTL-CNN are explored. Firstly, the task weights λ_1 and λ_2 are gradually adjusted between 0.2 and 1.2 in steps of 0.2, while other parameters remain constant. The total monitoring loss under different combination of λ_1 and λ_2 is recorded in Fig. 6. The warmer the color, the higher the monitoring loss. It is clearly visible that in the top range (0.9-1.2) of λ_1, the total monitoring loss is relatively high for the almost entire range of λ_2. When the value of λ_1 is around 0.8 and λ_2 in the range of (0.5-0.9), good performance can be obtained. The low monitoring loss value can also be achieved when λ_1 in the bottom range of (0.2-0.5) and λ_2 in the range of (0.2-0.3) or (0.6-1.2). This demonstrates that task weights do have a remarkable effect on the overall performance of the MTL-CNN. Therefore, it is necessary to achieve a balance between each

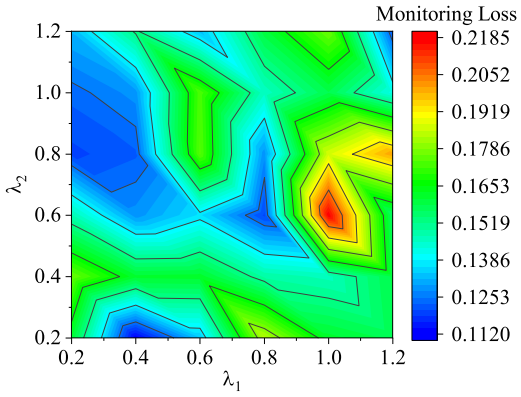

Fig. 6. The heatmap of monitoring loss under different task weights values of λ_1 and λ_2.

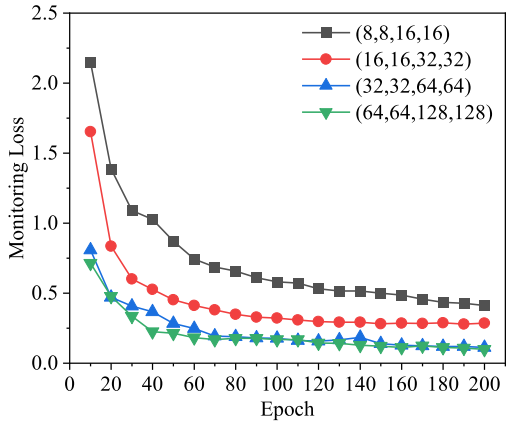

Fig. 7. The monitoring loss as a function of epochs for different model structures.

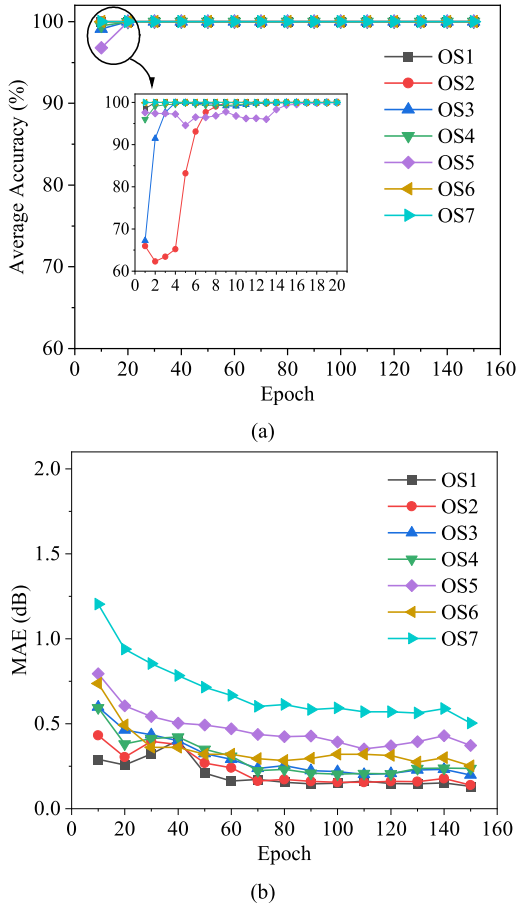

Fig. 8. (a) The OSR accuracy and (b) OSNR monitoring error as a function of epochs for different signals.

task to obtain the best comprehensive performance, rather than striving for the performance of a single task and ignoring the execution of another task.

Secondly, the effect of model structure on the performance of MTL-CNN is further investigated. The structure of the model is mainly determined by the number of convolutional kernels in each convolutional layer (C1, C2, C3, C4). The monitoring loss for different model structures: (8, 8, 16, 16), (16, 16, 32, 32), (32, 32, 64, 64), (64, 64, 128, 128) at different epochs has been recorded in Fig. 7. It is clear that the monitoring loss for all four model structures decreases as the number of epochs increases, in other words as the level of training deepens. With the network scale gradually increasing from (8, 8, 16, 16) and (16, 16, 32, 32) to (32, 32, 64, 64), the monitoring loss is becoming smaller and smaller. But when the network scale continues to extend to (64, 64, 128, 128), there is no significant improvement in the monitoring loss value and the number of model parameters increases sharply due to the increasing size of the network. According to the above analysis, it is crucial to select appropriate task weights and design a reasonable model structure for a given situation. For the case of this paper, the values of λ_1 and λ_2 are set to 0.4 and 0.2, respectively, and the model structure (32, 32, 64, 64) is a practical and reasonable option.

After determining the task weights and model structure, the analysis reveals that the monitoring loss of the model gradually converges with increasing epoch, which means that the performance of the model becomes more stable. In order to reduce the training time while ensuring the performance of the model, we determine that the model satisfies the above needs after 150 epochs. Then, the impact of the number of epochs on the performance is analyzed. The OSR and OSNR monitoring results at different epochs are shown in Fig. 8. In general, the overall recognition accuracies of the seven signals increase with the growth of epochs. The trained MTL-CNN at different epochs presents different recognition capabilities. In the initial stage, as shown in the inset of Fig. 8(a), the main reason for the recognition error at this point is that the spectrums of OS2 and OS3 are easily confused. As mentioned in section 2.1, modulation format, baud rate, and pulse shape determine the optical spectrum. Although the baud rate of OS2 is lower than that of OS3, pulse shaping of the 50% RZ broadens the spectrum to some extent compared to the NRZ, so that the spectrum of OS2 is somewhat similar to OS3. Additionally, the adjustment of model parameters is not finished due to the limited epochs, resulting in comparably low accuracies. As the epochs grow, the parameters are further tuned and the learning ability of MTL-CNN is enhanced, contributing to the gradually

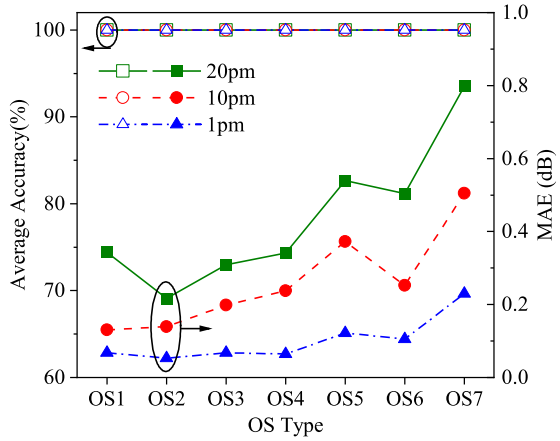

Fig. 9. The OSR accuracy and OSNR monitoring error for different signals with 20, 10 and 1 pm resolutions.

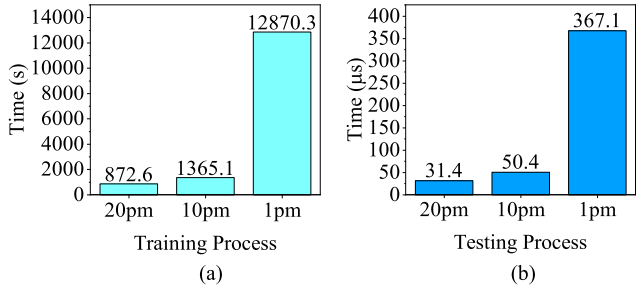

Fig. 10. (a) Training time and (b) Testing time of MTL-CNN models with 20, 10 and 1 pm resolutions.

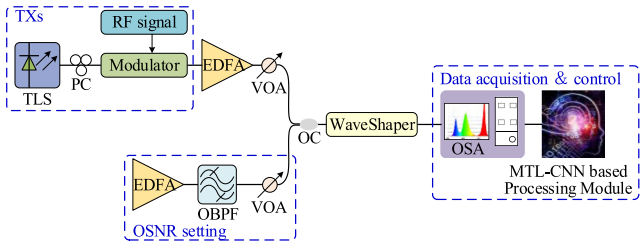

Fig. 11. Experimental setup for the proposed OSR and OSNR monitoring method. .

increased recognition accuracy. When the epochs arrive at 20, the recognition accuracies of the seven signals all attain 100% and will maintain the error-free results. As depicted in Fig. 8(b), it is seen that the MAE of the OSNR monitoring for the seven signals shows a general trend of gradually decreasing as the number of epochs increases. Similar to the OSR process, the overall OSNR monitoring error is larger in the initial stage because the optimization of the whole model parameters is not yet completed, except that OSR only needs 20 epochs to realize accurate recognition, whereas OSNR monitoring requires longer training time to achieve a low error monitoring. This suggests that compared with OSR, OSNR monitoring with low error is more difficult to perform. In addition, advanced modulation format signals (such as 64QAM, etc.) have a suboptimal monitoring performance compared to OOK and BPSK. But when epochs arrive at 150, the monitoring error of 64QAM can also reach 0.5 dB magnitude, which is an acceptable result.

The above simulation results are based on the optical spectrums with 10 pm resolution, which can be easily achieved by a conventional OSA. In this paper, we also use optical spectrums with 20 pm and 1 pm resolutions under test, to explore the impact of different spectrum resolutions on the performance of MTL-CNN. After 180, 150 and 130 epochs, respectively, the recognition accuracy and OSNR monitoring error results for the seven signals with 20, 10 and 1 pm resolutions are obtained, as shown in Fig. 9. The red curves marked with triangles illustrate the recognition accuracy and the blue curves marked with triangles illustrate the MAE of OSNR monitoring. With a spectrum resolution of 10 pm, we can realize accurate recognition of the seven signals to be measured in the presence of a variety of distortions. The MAEs of OSNR monitoring for the seven signals are 0.131, 0.139, 0.198, 0.237, 0.372, 0.252, 0.504 dB, respectively, and the overall monitoring error is 0.262 dB. With a spectrum resolution of 1 pm, we get a similar result: both the classification task and the regression task are performed very well. The difference is that optical spectrums with 1 pm resolution can provide more detailed features for model extraction and learning, reducing the number of epochs for accurate identification from 20 to 6 and the OSNR monitoring error from 0.262dB to 0.101dB. In the 20 pm case, the OSNR monitoring performance degrades to 0.436 dB. But accurate OSR can also be achieved.

Due to the dynamic and flexible characteristics of the network, it is important to pay attention not only to the accuracy of monitoring, but also to the overall time consumption, especially the testing time. Just as summarized in Fig. 10, we calculate both the training time and testing time for models with different spectrum resolutions based on an ordinary computer (Intel Core i5-8250 CPU and 8.00 GB RAM). The improvement in spectrum resolution from 10 pm to 1 pm provides more detailed features, however the amount of optical spectrum data has increased significantly, making each epoch more time-consuming. The total training time of the MTL-CNN model with a spectrum resolution of 1 pm is 12870.3 s, which is far more than 872.6 s and 1365.1 s corresponding to the 20 pm and 10 pm scenarios. With regard to testing time, it takes 31.4, 50.4 and 367.1 μs for a set of optical spectrum data under test to be analyzed by the MTL-CNN model with a spectrum resolution of 20, 10 and 1 pm, respectively. Although the MTL-CNN model with a spectrum resolution of 1 pm has slightly improved task execution performance, it comes at the cost of paying more in training time and testing time.

This demonstrates that our method is efficient and has an acceptable processing speed. It has the feasibility to be used for a fast real-time monitoring. It can be inferred that our scheme can achieve good performance under conventional spectrum resolution and has practical application value.

IV. Experimental Setup and Results

To further demonstrate the feasibility of our method, proof-of-concept experiments are carried out as shown in Fig. 11.

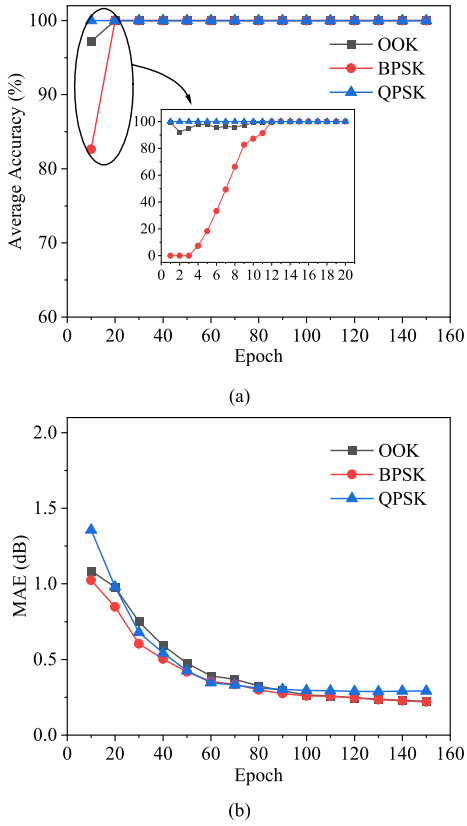

Fig. 12. (a) The OSR accuracy and (b) OSNR monitoring error as a function of epochs for different signals in the experiment.

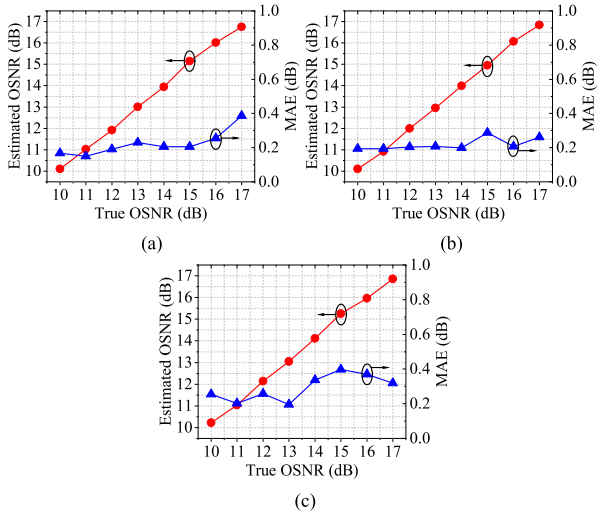

Fig. 13. Experimental results for OSNR monitoring: (a) OOK; (b) BPSK and (c) QPSK.

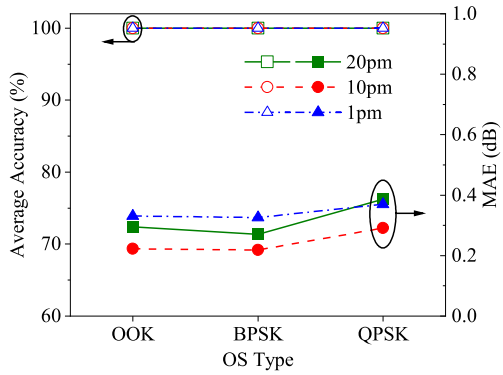

Fig. 14. The OSR accuracy and OSNR monitoring error for different signals in the experiment with 20, 10 and 1 pm resolutions.

The tunable laser source (TLS, Alnair Labs TLG-200) with a linewidth of less than 100 kHz is used to generate the laser. The center wavelength is set to 1550 nm and ± 1.25 GHz LFD is also formed by fine-tuning the TLS. The state of polarization of signal is appropriately adjusted by a polarization controller (PC) to match the polarization axis of the modulator. The suitable modulator and RF signal are used to get 10 Gbaud NRZ-OOK, NRZ-BPSK, and 11.3 Gbaud NRZ-QPSK signals. Through an EDFA and VOA, the power of the generated signal is set to 0 dBm. In the lower branch, ASE noise is produced by an EDFA and OBPF. With the assistance of a VOA, the received OSNR is adjusted from 10 to 17 dB in steps of 1 dB. At the receiver end, a Finisar WaveShaper 4000s tunable filter is utilized to form FS and FT in the range of -2 to 2 GHz in steps of 2 GHz. Finally, optical spectrums are collected by the high-resolution OSA based on stimulated Brillouin scattering (SBS) whose spectrum resolution is up to 0.1 pm [32]. Cost-effective optical spectrum acquisition can also be easily realized by using a widely tunable OBPF and a low-speed photodiode [22], [23]. By pre-processing, 2592 experiment samples for the above three signals are obtained for subsequent MTL-CNN model training and testing. After optimization, the MTL-CNN used in the experiment has the model structure of (32, 32, 64, 64) and its task weights are chosen as 1.0 and 0.4, respectively.

After 150 epochs, the overall performance of the model constructed for spectrums with 10 pm resolution is gradually stabilized. And the OSR and OSNR monitoring results are shown in Fig. 12. In common with simulation results, the model can accurately recognize the three signal spectrums generated by the experiment. In the initial stage, BPSK signals are easily confused with OOK signals rather than QPSK signals because the former two have the same MLW, while the latter has the largest MLW. Besides, due to the non-ideal characteristics of the modulator used in the experiment, BPSK signals will have spectral lines similar to the OOK signals. But it only takes 13 epochs to make a big difference, as shown in the inset of Fig. 12(a). The OSNR monitoring error for the three signals decreases as the number of epochs increases as depicted in Fig. 12(b). The MAEs of OSNR monitoring for OOK, BPSK, and QPSK signals are 0.223, 0.219, 0.291 dB, respectively. The detailed OSNR estimation results are shown in Fig. 13. The red curves marked with circles denote the averaged value of estimated OSNR and the blue curves marked with triangles denote MAE at each OSNR value. The maximum MAE at each OSNR value for OOK, BPSK, and QPSK signals are 0.385, 0.287, and 0.396 dB, respectively.

In the experiment, optical spectrums with 20 pm and 1 pm resolutions for the above three signals are also acquired. The results at different resolutions are shown for comparison in Fig. 14. The

proposed method can achieve accurate recognition of all three signals, and the overall OSNR monitoring error is 0.317, 0.244 and 0.342 dB with a spectrum resolution of 20, 10 and 1 pm, respectively. The error obtained in the experiment is slightly higher than that obtained in the simulation for optical spectrums with 1 pm resolution, mainly because the number of experiment samples is much smaller than that of simulation samples, making the features not fully learned. It is important that the error of each OSNR estimation is kept within 0.4 dB for all three signals, which facilitates a high level of reliability in OSNR monitoring. The training time is 147.2, 159.3 and 1708.5 s with a spectrum resolution of 20, 10 and 1 pm, respectively. Correspondingly, the testing time is 42.3, 65.3 and 420.1 μs. The above results prove that our scheme can realize good performance at the resolution level that a conventional OSA can achieve. The experimental results, which are consistent with the simulation results, further demonstrate the effectiveness of our method.

V. Conclusion

In this paper, we have proposed a MTL-CNN technique combined with optical spectrums for simultaneous OSR and OSNR monitoring. It effectively solves the problem that the traditional dual-stage scheme cannot realize multiple parameters monitoring at the same time. The results suggest that our method can achieve high accuracy in OSR and low error in OSNR monitoring for seven commonly used signals. The recognition accuracy and MAE of OSNR monitoring are 100%, 0.262 dB in the simulation system, and 100%, 0.244 dB in the experiment system with a spectrum resolution of 10 pm. Similar results can also be achieved with a spectrum resolution of 20 pm and 1 pm. To be specific, with the help of a conventional OSA, the proposed method can achieve relatively good monitoring performance with low time consumption. Additionally, it is robust to various distortions and inherently insensitive to CD and PMD. Therefore, it provides a new approach to efficiently improve the stability and reliability of the future elastic and cognitive optical network.

References

[1] K. Christodoulopoulos, I. Tomkos, and E. A. Varvarigos, "Elastic bandwidth allocation in flexible OFDM-based optical networks," *J. Lightw. Technol.*, vol. 29, no. 9, pp. 1354–1366, May 2011.

[2] O. Gerstel, M. Jinno, A. Lord, and S. J. B. Yoo, "Elastic optical networking: A new dawn for the optical layer?," *IEEE Commun. Mag.*, vol. 50, no. 2, pp. s12–s20, Feb. 2012.

[3] X. Lin, O. A. Dobre, T. M. Ngatched, Y. A. Eldemerdash, and C. Li, "Joint modulation classification and OSNR estimation enabled by support vector machine," *IEEE Photon. Technol. Lett.*, vol. 30, no. 24, pp. 2127–2130, Dec. 2018.

[4] Y. Li, N. Hua, and J. Li, "Optical spectrum feature analysis and recognition for optical network security with machine learning," *Opt. Exp.*, vol. 27, no. 17, pp. 24808–24827, 2019.

[5] X. Sun *et al.*, "Monitoring of OSNR using an improved binary particle swarm optimization and deep neural network in coherent optical systems," *Photonics*, vol. 6, no. 4, pp. 111–128, 2019.

[6] L. Xia, J. Zhang, S. Hu, M. Zhu, Y. Song, and K. Qiu, "Transfer learning assisted deep neural network for osnr estimation," *Opt. Exp.*, vol. 27, no. 14, pp. 19398–19406, 2019.

[7] C. K. Chan, *Optical Performance Monitoring: Advanced Techniques For Next-Generation Photonic Networks*, Amsterdam, The Netherlands: Elsevier, 2010.

[8] Z. Yang *et al.*, "Unsupervised neural network for modulation format discrimination and identification," *IEEE Access*, vol. 7, pp. 7077–7070, 2019.

[9] V. S. Ghayal and R. Jeyachitra, "Efficient eye diagram analyzer for optical modulation format recognition using deep learning technique," in *Proc. Adv. Elect. Comput. Technol.*, 2020, pp. 655–666.

[10] W. Zhang *et al.*, "Identifying probabilistically shaped modulation formats through 2D stokes planes with two-stage deep neural networks," *IEEE Access*, vol. 8, pp. 6742–6750, 2020.

[11] X. Fan *et al.*, "Joint optical performance monitoring and modulation format/bit-rate identification by CNN-based multi-task learning," *IEEE Photon. J.*, vol. 10, no. 5, pp. 1–13, Oct. 2018.

[12] F. N. Khan *et al.*, "Experimental demonstration of joint OSNR monitoring and modulation format identification using asynchronous single channel sampling," *Opt. Exp.*, vol. 23, no. 23, pp. 30337–30346, 2015.

[13] H. J. Cho *et al.*, "Convolutional recurrent machine learning for OSNR and launch power estimation: A critical assessment," in *Proc. Opt. FiberCommun. Conf.*, 2020, Paper M2J.5.

[14] F. N. Khan *et al.*, "Joint OSNR monitoring and modulation format identification in digital coherent receivers using deep neural networks," *Opt. Exp.*, vol. 25, no. 15, pp. 17767–17776, 2017.

[15] A. Yi *et al.*, "Modulation format identification and osnr monitoring using density distributions in stokes axes for digital coherent receivers," *Opt. Exp.*, vol. 27, no. 4, pp. 4471–4479, Feb. 2019.

[16] H. Lu, S. Cui, C. Ke, and D. Liu, "Automatic reference optical spectrum retrieval method for ultra-high resolution optical spectrum distortion analysis utilizing integrated machine learning techniques," *Opt. Exp*, vol. 25, no. 26, pp. 32491–32503, Dec. 2017.

[17] Q. Xiang, Y. Yang, Q. Zhang, and Y. Yao, "Joint and accurate OSNR estimation and modulation format identification scheme using the feature-based ANN," *IEEE Photon. J.*, vol. 11, no. 4, pp. 1–11, Aug. 2019.

[18] G. Yin, S. Cui, C. Ke, and D. Liu, "Reference optical spectrum based in-band OSNR monitoring method for EDFA amplified multispan optical fiber transmission system with cascaded filtering effect," *IEEE Photon. J.*, vol. 10, no. 3, pp. 1–10, Jun. 2018.

[19] Y. Zhong *et al.*, "Impact of out-of-band noise on OSNR measurement using brillouin optical spectrum analyzer and its mitigation method," *IEEE Photon. J.*, vol. 10, no. 5, pp. 1–10, Sep. 2018.

[20] Y. Zhong *et al.*, "A robust reference optical spectrum based in-Band OSNR monitoring method suitable for flexible optical networks," *IEEE Photon. J.*, vol. 12, no. 3, pp. 1–10, Jun. 2020.

[21] D. Wang *et al.*, "Machine learning-based multifunctional optical spectrum analysis technique," *IEEE Access*, vol. 7, pp. 19726–19737, 2019.

[22] C. Hu, W. Li, H. Zheng, Q. Feng, Q. Zheng, and Y. Wang,, "A novel cost-effective and distributed in-band OSNR monitoring method using gaussian process regression," *IEEE Photon. J.*, vol. 11, no. 4, pp. 1–12, Aug. 2019.

[23] C. Hu *et al.*, "Modulation-format-independent in-band OSNR monitoring technique using Gaussian process regression for a Raman amplified multi-span system with a cascaded filtering effect," *Opt. Exp.*, vol. 28, no. 7, pp. 10134–10144, 2020.

[24] E. Ip and J. M. Kahn, "Power spectra of return-to-zero optical signals," *J. Lightw. Technol.*, vol. 24, no. 3, pp. 1610–1618, Mar. 2006.

[25] Z. Dong *et al.*, "Modulation-format-independent OSNR monitoring insensitive to cascaded filtering effects by low-cost coherent receptions and RF power measurements," *Opt. Exp*, vol. 23, no. 12, pp. 15971–15982, Jun. 2015.

[26] R. Caruana, "Multitask learning," *Mach. Learn.*, vol. 28, no. 1, pp. 41–75, 1997.

[27] M. Long, Z. Cao, J. Wang, and S. Y. Philip, "Learning multiple tasks with multilinear relationship networks," in *Proc. Adv. Neural Inf. Process. Syst.*, 2017, pp. 1594–1603.

[28] S. Ruder, "An overview of multi-task learning in deep neural networks," 2017, *arXiv:1706.05098*. [Online]. Available: http://arxiv.org/abs/1706.05098

[29] A. G. Howard *et al.*, "Mobilenets: Efficient convolutional neural networks for mobile vision applications," Apr. 2017, *arXiv:1704.04861*.

[30] Y. Zhang *et al.*, "Eye diagram measurement-based joint modulation format, OSNR, ROF, and skew monitoring of coherent channel using deep learning," *J. Lightw. Technol.*, vol. 37, no. 23, pp. 5907–5913, Dec. 2019.

[31] A. Gulli and S. Pal, *Deep Learning with Keras*, Birmingham. U.K.: Packt Publishing Ltd., 2017.

[32] C. Xing, C. Ke, K. Zhang, Z. Guo, Y. Zhong, and D. Liu, "Polarization- and wavelength-independent SBS-based filters for high resolution optical spectrum measurement," *Opt. Exp.*, vol. 25, no. 18, pp. 20969–20982, 2017.